



<https://doi.org/10.31217/p.39.1.10>

Modified Floater of Heaving Device Wave Energy Converter (WEC): An Experimental and Numerical Study

Dendy Satrio^{1*}, Febri Budihantono¹, Mohammad Farid¹, Nik Ahmad Ridhwan², Maktum Muharja¹, Muhammad Luqman Hakim³, Tuswan³, Dandun Mahesa Prabowoputra⁴, Fuad Mahfud Assidiq⁵, Wahyu Nur Fadilah⁶

¹ Institut Teknologi Sepuluh Nopember, Surabaya 60111, Jawa Timur, Indonesia

² Universiti Teknologi Malaysia, Johor Bahru 81310, Johor, Malaysia

³ Universitas Diponegoro, Semarang 50275, Jawa Tengah, Indonesia

⁴ Universitas Jenderal Soedirman, Purwokerto 53122, Jawa Tengah, Indonesia

⁵ Universitas Hasanuddin, Gowa 92171, Sulawesi Selatan, Indonesia

⁶ Politeknik Elektronika Negeri Surabaya, Surabaya 60111, Jawa Timur, Indonesia

* Corresponding author (e-mail: dendy.satrio@its.ac.id)

ARTICLE INFO

Original scientific paper

Received 10 December 2024

Accepted 4 March 2025

Key words:

Ocean renewable energy
Wave energy converter
Heaving device
Towing tank
Boundary element method

ABSTRACT

Indonesia has a population nearing 300 million and an electricity consumption of 1,285 kWh per capita. However, Mentawai Waters which is surrounded by wave energy potential, still has 23 out of 43 villages off-grid. This study examines energy extraction in Mentawai Waters using a Wave Energy Converter (WEC) with a heaving device mechanism. It focuses on measuring heaving motion, and excitation force, and calculating power and energy production. The heaving WEC device type is selected for its suitability with the local environmental characteristics. The most important of which are wave heights reaching 2.3 m and periods reaching 8.3 s. A combination of experimental testing using the Towing Tank Laboratory and numerical methods with the Boundary Element Method (BEM) is used to optimize the results. The tests focus on six variations of floater diameters ranging from 23 to 33 cm, under wave heights of 0.04 to 0.08 m, with wave periods ranging from 0.6 s to 2.6 s. Both methods indicate that the 29 cm diameter (Floater Type 2) is the most optimal variation, with an average mechanical power output of 446 watts, which is 26.17% higher than Floater Type 1. At a 1:1 scale, an array of 10 Floater Type 2 WECs, with a maximum annual energy output of 35,226 kWh, confirms the point absorber as a suitable WEC type for Mentawai Waters, capable of illuminating key areas, including public facilities.

1 Introduction

Indonesia's population experiences growth every year. As evidenced by projected data from the Central Bureau of Statistics in 2030 Indonesia's population will amount to 296 million people [1]. As the population increases, there will be an increase in national electricity demand. In 2023, the national electricity demand is 1,285 kWh/capita [2]. Meanwhile, after projections, electricity demand in 2030 is predicted to increase to 1,440 kWh/capita. In addition, exhaust gas emissions are also a problem because in 2020 carbon gas emissions in Indonesia

amounted to 543 million tons of CO₂. The largest contribution to the disposal of carbon gas emissions is 51% from power plants, 24% from motor vehicles, 19% from industry, and the rest from other sectors [3].

The potential of renewable energy sources needs to be effectively harnessed to meet national electricity demands and reduce carbon emissions from conventional power plants. One of the most significant renewable energy sources in Indonesia is ocean energy. In West Sumatra, there is substantial potential in the wave energy sector, with significant wave heights predominantly ranging from 1.4 to 2.3 meters and wave periods rang-

ing between 7.8 and 8.3 seconds representing 35% of the total annual wave events. These data were based on secondary data of annual significant wave events and the outcomes of wave distribution modeling in Mentawai Waters [3]. The Mentawai Waters contain a potential of 171.6 kW and the Bengkulu Waters contain a potential of 101.26 kW. This shows that Indonesia has a large wave energy potential [5].

Unfortunately, wave power generation has not been developed as much as ocean current power generation [6], [7], [8]. When implemented at sea, research on material type selection [9], [10], [11] is no less important than research on performance. The technology Readiness Level (TRL) of wave power generation is still relatively low when compared to ocean current extraction technology, namely between 6 and 7 [12], [13], [14]. Numerous studies have been conducted to improve the TRL, including prior research using experimental methods that focused on floater heights in WEC technology with a heaving device [15]. The best scenario from the study, which achieved a performance increase of up to 1.1%, was further explored in this research as a continuation of the previous experiment.

Hydrodynamic coefficients of the WEC heaving device type can be calculated using BEM to obtain several coefficients such as excitation force magnitude and mechanical power. This method was utilized in previous research to investigate two Point Absorber designs using WaveAnalysisMIT (WAMIT) software combined with experimental methods. The 1:25 scale model was referenced by Powerbuoy and Wavebob [16]. A Point Absorber with a large heave plate or a heavier plate produces a lower natural frequency, allowing for better power generation in small periods [17]. In continuing the investigation of the effect of viscosity using the BEM, the Finite Volume Method (FVM) has been employed to determine the damping coefficient, which is not obtained from the BEM approach [18]. Additionally, experimental methods were employed to complement this

study, using models based on established references [16]. Findings indicate that point absorbers can extract up to 27% of the total available power.

The performance of floaters in generating mechanical power can be evaluated through experimental methods [16][19]. To compare and validate the results, this study employed both experimental and numerical analysis using BEM. The testing model dimensions were follow those used in earlier studies to further explore the readiness of the technology [15]. The selected floater height was 8 cm, as it demonstrated the best performance in previous tests. The complexity of this testing is essential to produce valid results, thereby contributing to the enhancement of the TRL of the relevant technology.

2 Material and Methods

2.1 Technology Assessment

2.1.1 Resource Assessment

A study in 2017 identified several potential locations for harnessing wave energy across Indonesia, as shown in Figure 1 [20]. Among the nine identified sites, the Mentawai Waters stands out as one of the key areas, marked with the letter "D". The Mentawai Islands, located off the western coast of Sumatra and facing the Indian Ocean, offer a highly favorable environment for WEC.

Two primary wave characteristics in this region support its energy potential, regular wave clumps with a consistent height of 1-2 meters throughout the year, and larger swell waves with wavelengths up to 100 meters and periods ranging from 0.9 to 15 seconds [21]. These natural conditions make the Mentawai Waters an ideal location for exploring wave energy generation. The wave characteristics in the Mentawai region present an untapped opportunity to address local energy shortages, which are further detailed in Table 1.

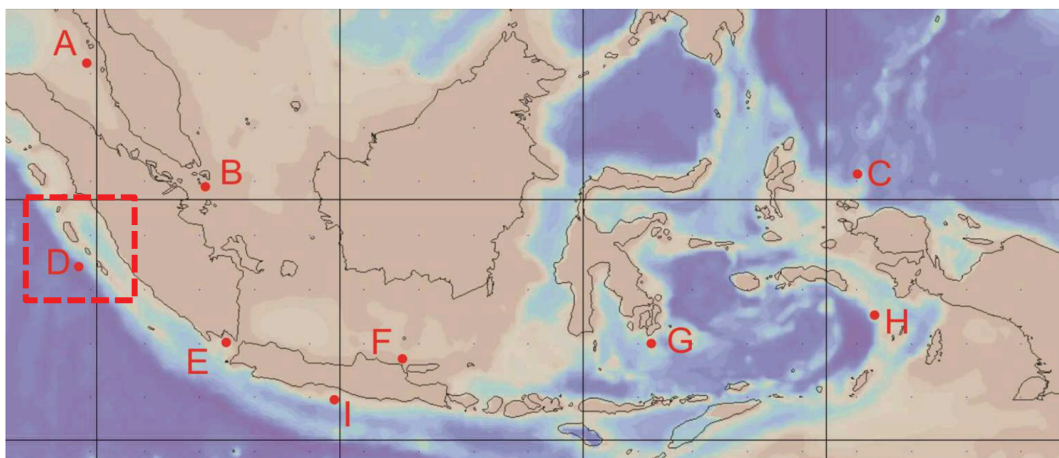


Figure 1 The location of wave energy potential in Indonesia seas: Mentawai Waters [20]

Table 1 Mentawai Waters characteristics [4], [15], [22].

Symbol	Parameters	Description
d	Depth	30 – 200 m
-	Coordinates	98°35' – 100°32' E and 0°55' – 3°21'S
-	Region	Offshore
H_s	Wave height	0.5 – 2.3 m
T	Wave period	7.8 – 8.3 s
P	Power	The average annual wave power is about 8 – 16 kW/m with a maximum power of 16 – 20 kW/m
f	Frequency of occurrence	35% total frequency of annual wave events

2.1.2 Wave Energy Converter Assessment

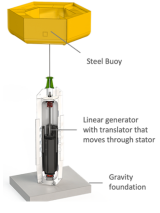
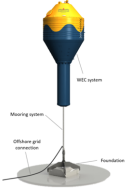
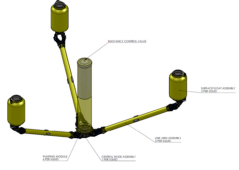

This research focuses on WEC that utilize heaving devices using the Point Absorber Power Take-Off (PTO) mechanism, a common type within the Oscillating Body System (OBS) classification. Heaving device point absorbers harness the vertical motion caused by ocean waves to drive a PTO system, converting wave energy into electrical power [23]. As outlined by [23] and [24] point absorbers are highly effective, particularly due to their simplicity and capacity to function in various sea states.

Factors such as wave height (H_s), period (T) and depth must be carefully considered when designing these

devices to ensure optimal energy capture [17]. The adaptability of point absorbers to local environmental conditions is critical to maximize energy output. Point Absorbers that exhibit this heaving mechanism, are often chosen for their straightforward design and potential for high efficiency in various geographical locations [23], [25], [26]. Table 2 provides an overview of various WECs utilizing point absorber mechanisms for PTO, highlighting potential options for efficient wave energy extraction.

The Seabased S2.7 wave energy converter is a floating device designed to harness energy from wave height ranging between 2 to 7 meters, with wave periods from 10.5 to 11 seconds. It operates in water depths exceed-

Table 2 Various types of heaving device WECs.

References	WEC Devices	Type	TRL	d (m):	H_s (m):	T (s):	P Produced (kW)
<i>Seabased S2.7 wave energy converter</i> [27], [28], [29], [30]		Floating	9	> 50	2 – 7	10.5 – 11	10 – 30
<i>WEC C4 by CorPower</i> [31], [32]		Floating	9	> 40	0.25 – 8	4.16 – 24.16	300
<i>WaveNET SQUID, Albatern Wave Energy Ltd</i> [28], [33], [34]		Floating	8	20 – 150	0.3 – 6	9.5 – 10.5	75
<i>OPT PowerBuoy®</i> [25], [35], [36]		Floating	9	30 – 3,000	1 – 5	7.6 – 22.3	40 – 500

ing 50 meters and produces between 10 to 30 kW of power per unit. This technology is well-suited for array deployment, allowing for scalability to meet larger energy demands.

The WEC C4 by CorPower is another advanced floating point absorber device, with a high TRL of 9, indicating its near-commercial development status. This WEC operates in depths of over 40 meters and captures wave energy from height ranging between 0.25 and 8 meters. It operates efficiently in wave periods ranging from 4.16 to 24.16 seconds, producing up to 300 kW of power per unit. CorPower's technology focuses on maximizing energy extraction through advanced control systems, and it is well-suited for regions with diverse sea states, making it adaptable to various marine conditions.

The WaveNET SQUID, developed by Albatern Wave Energy Ltd, is a floating WEC that functions in water depths ranging from 20 to 150 meters. It captures energy from waves with height between 0.3 and 6 meters, with wave periods from 9.5 to 10.5 seconds, producing 75 kW of power. This system is also designed for array configuration, improving its overall energy production capacity when deployed in larger setups.

The OPT PowerBuoy designed for operation across a wide range of water depths, from 30 to 3,000 meters, is the most versatile among these devices. It captures energy from waves with height of 1 to 5 meters and wave periods between 7.6 to 23.3 seconds. With a power production range of 40 to 500 kW per unit, this device demonstrates significant flexibility and scalability for varying marine environments. Its ability to perform in deep

waters makes it a particularly viable solution for regions like the Mentawai Islands, which face deep-water challenges yet hold vast potential for wave energy extraction.

Based on the analysis, the OPT PowerBuoy was selected as the most suitable WEC for deployment in the Mentawai Islands. This choice was made due to several factors aligning with the region's deep-water characteristics. The floating design of the OPT PowerBuoy allows it to operate efficiently across depths ranging from 30 to 3,000 meters, ensuring flexibility in diverse marine conditions [26], [35]

Additionally, it offers a robust power output ranging from 40 to 500 kW, making it capable of capturing significant wave energy in the open ocean [25]. This high output, combined with its proven ability to perform under varying wave heights and periods, solidifies its selection as the most optimal solution for wave energy extraction in this study [23], [24].

2.2 Experimental Method

2.2.1 Physical Model Geometry

The geometry data for the Point Absorber used in this study, both in experimental and numerical testing, was sourced from prior research. An earlier study noted that the geometry was scaled down using a 1:10 ratio of the PowerBuoy developed by Ocean Power Technologies [15], [16]. The illustration of the model to be used in the experimental testing is shown in Figure 2, and each parameter is further explained in Table 3.

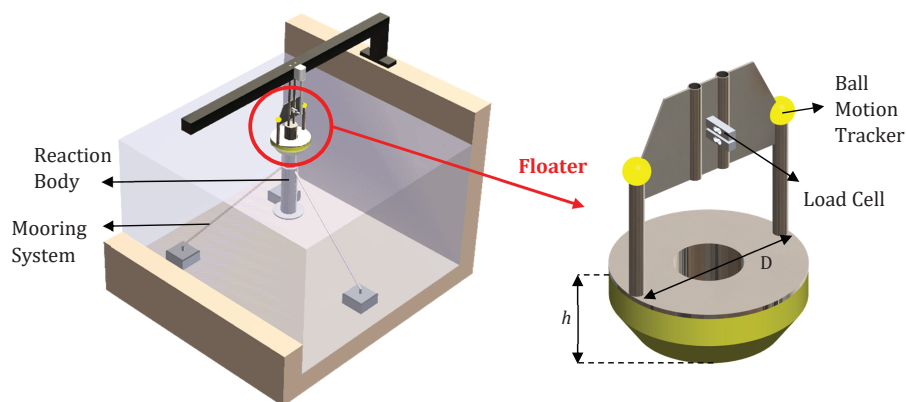


Figure 2 The design model of heaving device WEC [15].

Table 3 Detail specifications of the physical model.

Component	Symbol	Value
Floater height	h	8 cm
Floater diameter	D_f	Floater Type 1 (27 cm)
		Floater Type 2 (29 cm)
Floater displacement	-	4.91 Kg
Floater material	Ethylene-vinyl acetate foam (EVA foam)	

As explained in Table 3, one of the variations in this study is the floater diameter. The floater with a diameter of 27 cm was referred to as Floater Type 1, while the floater with a diameter of 29 cm was referred to as Floater Type 2.

2.2.2 Experimental Setup

The test was carried out at Institut Teknologi Sepuluh Nopember (ITS), by using the ITS Hydrodynamics laboratory. The setup of the Towing Tank in this laboratory is depicted in Figure 3 and Figure 4. This laboratory has dimensions of 50 meters in length, 3 meters in width, and 2 meters in height, with a water depth of 1.95 meters. The wave generator utilized a plunger system capable of producing both regular and irregular waves. The maximum wave heights that can be generated are 0.3 meters for regular waves and 0.7 meters for irregular waves, with a wave period range of 0.5 to 3.0 seconds [8].

In this study, wave heights of 0.02 m, 0.03 m, and 0.04 m were utilized, along with wave periods of 0.6 s,

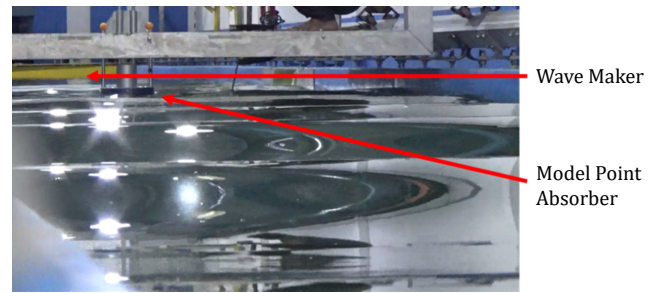


Figure 3 Towing Tank facilities with WEC physical model and instrumentations.

1 s, 1.4 s, 1.8 s, 2.2 s, and 2.6 s, using regular waves. The model was positioned 15 meters from the wave generator to ensure that the waves would reach the test object quickly. The illustration of this placement can be seen in Figure 4 (a) and (b) [15]. This study focused on variations in floater diameter (D_f), which are referred to as Floater Type 1 and Type 2, as shown in Table 3.

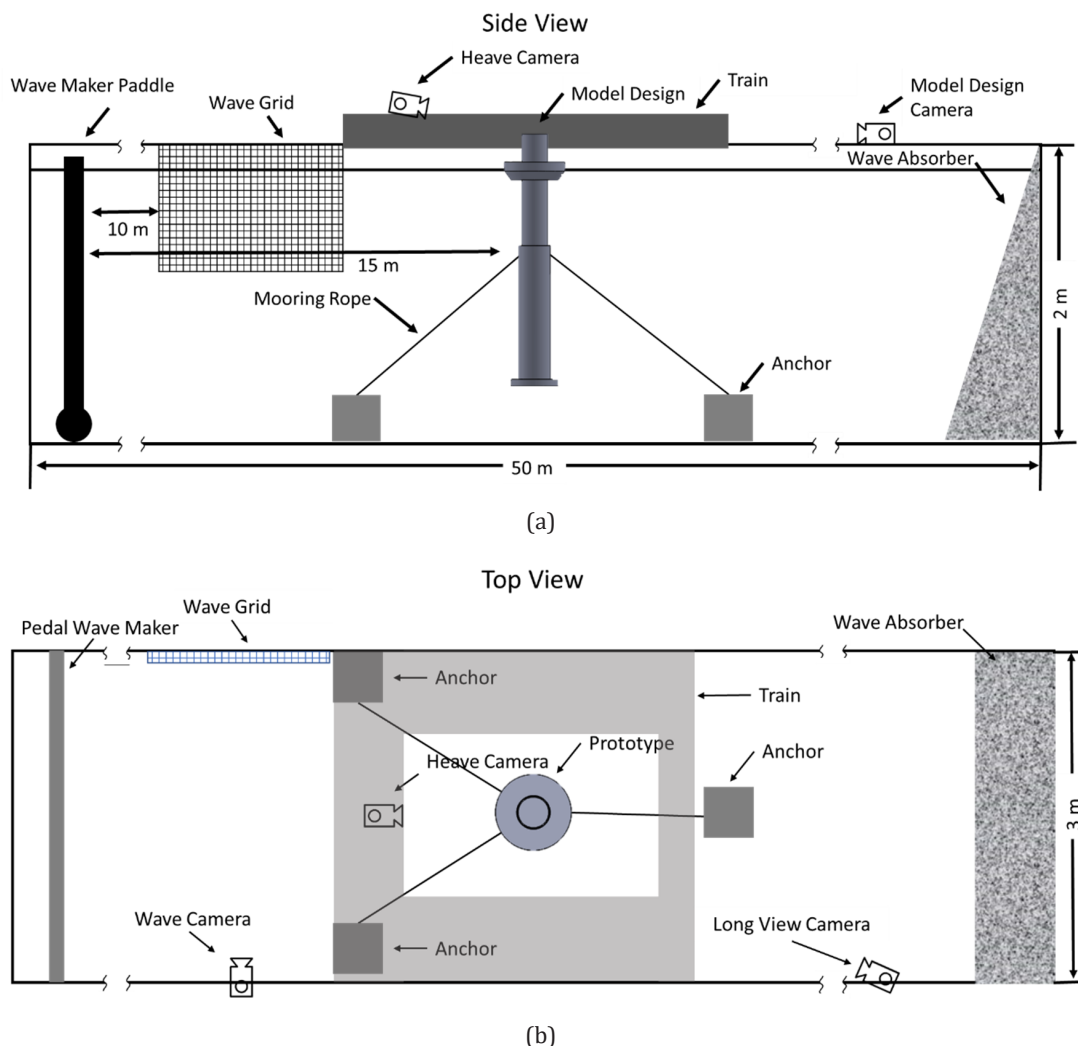


Figure 4 Schematic diagrams with (a) side view and (b) top view [15].

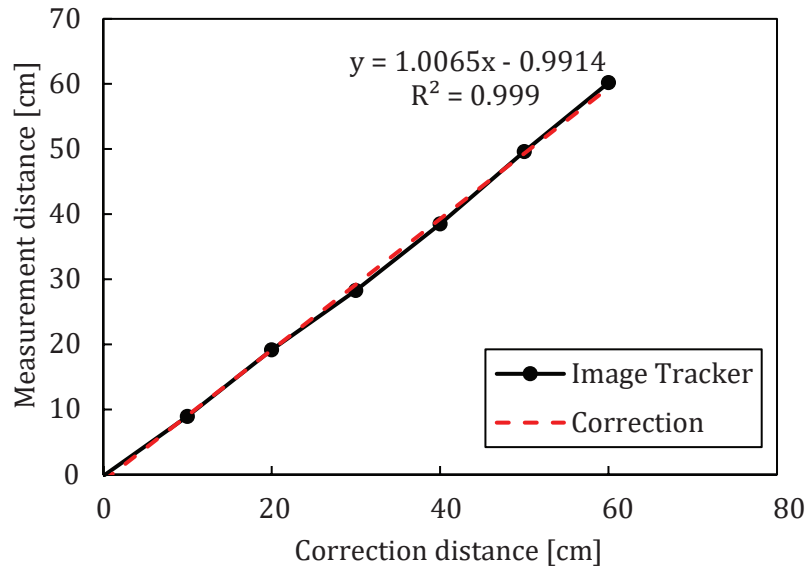


Figure 5 Heave motion instrument calibration.

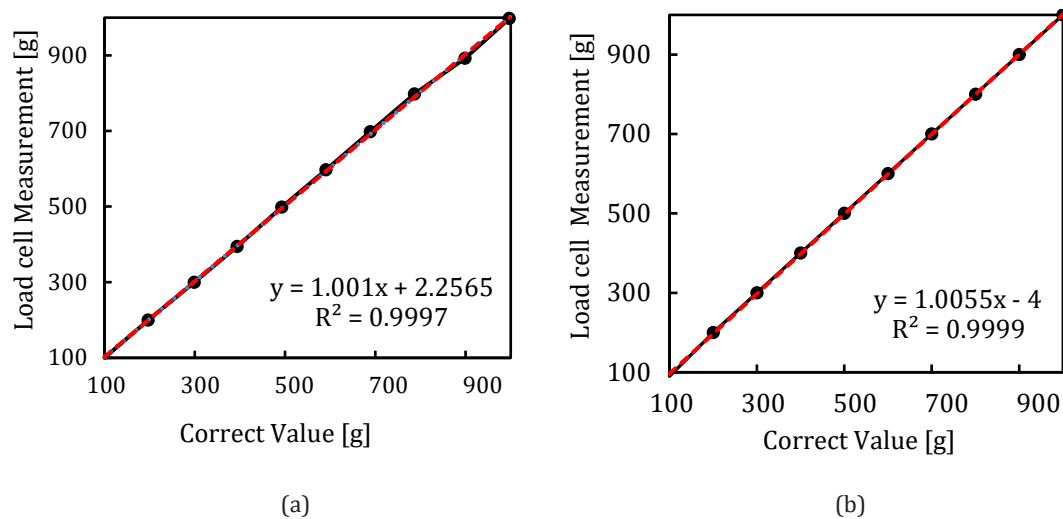


Figure 6 Load cell calibration in (a) Y+ axis and (b) Y- axis measurement.

2.2.3 Instruments Calibration

Instruments are crucial to measure mechanical power, excitation force, and heave motion in WEC. The first instrument calculated heave force through the integration of a camera and image tracking software. The camera detected the motion of a ball, as shown in Figure 2, and the software calculated its displacement to measure heave accurately.

The calibration process involved suspending an object that could be easily captured by the camera, with its position varying from 0 to 60 cm in 10 cm increments. Each movement was recorded by the camera and software, and the resulting data were compared to the intervals marked on the measuring tape. As shown in Figure 5, a correlation of 0.999 was achieved, indicating minimal error in the instrument.

The second instrument and calibration were conducted for the load cell sensor using weights ranging from 100 to 1000 grams in 100-gram increments. The weights were measured with a balance scale and then re-measured with the load cell. The calibration results, shown in Figure 6 (a) and (b), indicated strong correlations, with coefficients of 0.9999 for the Y+ direction and 0.9997 for the Y- direction, confirming the accuracy of the load cell sensor.

2.3 Numerical Method

2.3.1 Numerical Model Geometry

Numerical simulations were conducted using the BEM method with Ansys software and the Ansys Aqwa solver, based on model specifications matching the ex-

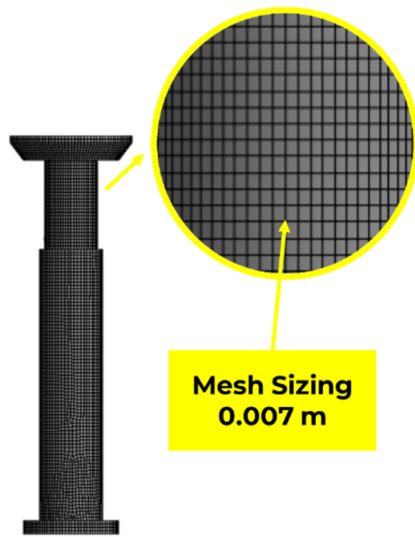


Figure 7 Numerical model geometry and meshing.

perimental setup. Additional variations in diameter, specifically 23 cm, 25 cm, 31 cm, and 33 cm, were included to perform an initial analysis of diameters closest to those used in the experiments, providing a basis for comparison and further evaluation.

To optimize the meshing process, some non-essential components like brackets, holders, and smaller parts of the spar were omitted. This adjustment aimed to improve simulation accuracy and efficiency. In the numerical model, only the submerged sections were included, as the hydrodynamic analysis in Ansys Aqwa focused solely on water-immersed components. The model used in this numerical simulation is shown in Figure 7.

2.3.2 Grid Independence Study

The meshing process significantly affected the accuracy of the simulation, as smaller mesh sizes and a higher number of meshes resulted in more accurate outcomes. In BEM simulation, a finer mesh also enabled the simulation to cover a wider range of wave frequen-

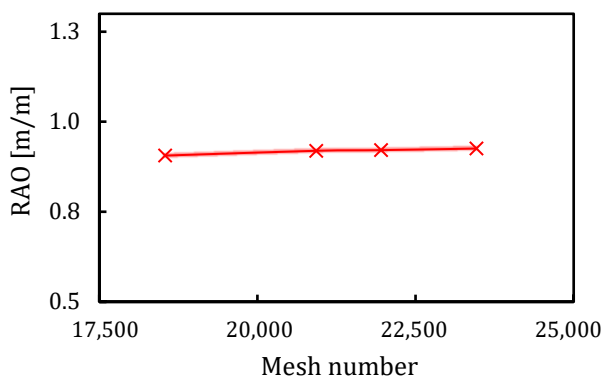


Figure 8 The grid independence study.

cies. A Mesh independence study was conducted by selecting a single Response Amplitude Operator (RAO) value and varying the mesh size through several grid experiments until the RAO value stabilized [19].

Testing began with a mesh count of 18,500, which was then gradually increased. When the mesh count reached approximately 23,500, a stable graph was achieved, as shown in Figure 8. This indicated that further increases in the number of meshes would not produce significant effects, while a higher mesh count would extend the simulation time. Therefore, a mesh count of 23,460 was chosen as a compromise between accuracy and computational efficiency.

2.4 Performance Parameters

2.4.1 Heaving Performance

Heaving performance can also be referred to as the floater's reaction RAO, and it is observed from the floater reaction above the wave-affected water surface. To obtain a value for one point on the RAO or performance heaving graph, an average must be taken for each wave period of the conversion process of experimental data into time series. The value of the wave's height will be divided by the average value of each wave period to generate a non-dimensional parameter value.

$$RAO(\omega) = \left(\frac{\zeta_a}{\zeta_w} \right) \quad (1)$$

$RAO(\omega)$ is the Response Amplitude Operator, which represents the ratio of the amplitude of motion of a structure to the amplitude of the incident wave at a given frequency (ω). In this formula, ζ_a denotes the amplitude of motion of the structure, while ζ_w refers to the amplitude of the incident wave. This relationship helps quantify the structure's response to wave forces, providing insight into how the system will react under different wave conditions.

2.4.2 Excitation Force and Relative Velocity

The translational equation follows Newton's second law and is written as:

$$m \cdot a = F \quad (2)$$

Equation (2) shows that F represents the total force acting on the body, where m is the mass, and a is the translational acceleration. In this study, the Floating Point Absorber device consisted of two main parts: a floater and a reaction body, connected via a linear mass-spring-damper system to simulate the PTO mechanism. The primary focus was on heaving motion, meaning the system operated with one degree of freedom. The equations of motion for each part of the system were reduced to the equation below:

$$\text{Floater} : m_F \cdot a_F = (F_z)_F + F_{PTO} \quad (3)$$

$$\text{Reacting Body} : m_R \cdot a_R = (F_z)_R - F_{PTO} \quad (4)$$

The subscripts F and R refer to the floater and reaction body respectively. The vertical force component, F_z , represents the heave force. The PTO force is modeled as a spring-damper system and is expressed as:

$$F_{PTO} = -c_{PTO} \cdot (U_F - U_R) - K_{PTO} \cdot (Z_F - Z_R) \quad (5)$$

Where K_{PTO} represents spring stiffness and C_{PTO} refers to the damping coefficient that governs power absorption. In contrast to conventional setups, our system replaced the PTO with a load cell to measure excitation forces. The primary objective here was to assess the dynamic behavior of the system, rather than focusing on energy extraction. The energy capture process, instead, was estimated through mathematical methods, with the average power output being derived by multiplying the PTO force by the instantaneous relative velocity, as demonstrated in equation (6) in the next section.

2.4.3 Mechanical Power and Energy

This study did not examine the generation of electrical energy in depth. But after finding the force of the floater and its displacement speed, it can be calculated the power generated through the following equation [4]:

$$P = P(t) = F_{pto}(t) \cdot U_r(t) \quad (6)$$

Where $P(t)$ is the mechanical power (watts), is the $F_{pto}(t)$ excitation force of the floater (Newtons), and is the relative speed of the floater ($U_r(t)$ m/s). To produce a non-dimensional value, it will be divided by the amplitude of the squared wave.

$$AEP = 8760 \cdot A_v \cdot P_{mean} \text{ (kWh)} \quad (7)$$

AEP represents the total energy output of a device over a full year. The figure of 8,760 hours corresponds to the total operational time in a year, based on continuous 24-hour daily operation. An availability factor (A_v) of 90% was applied, accounting for the proportion of time the device is expected to remain operational functional [37], [38]. In this approach, the average power was substituted with the average mechanical power output to provide a more precise calculation of annual energy production.

3 Results and Discussion

3.1 Experimental Method Results

Data retrieval was conducted by recording the model's movement, followed by importing the video into an image processing application. The movement data, cap-

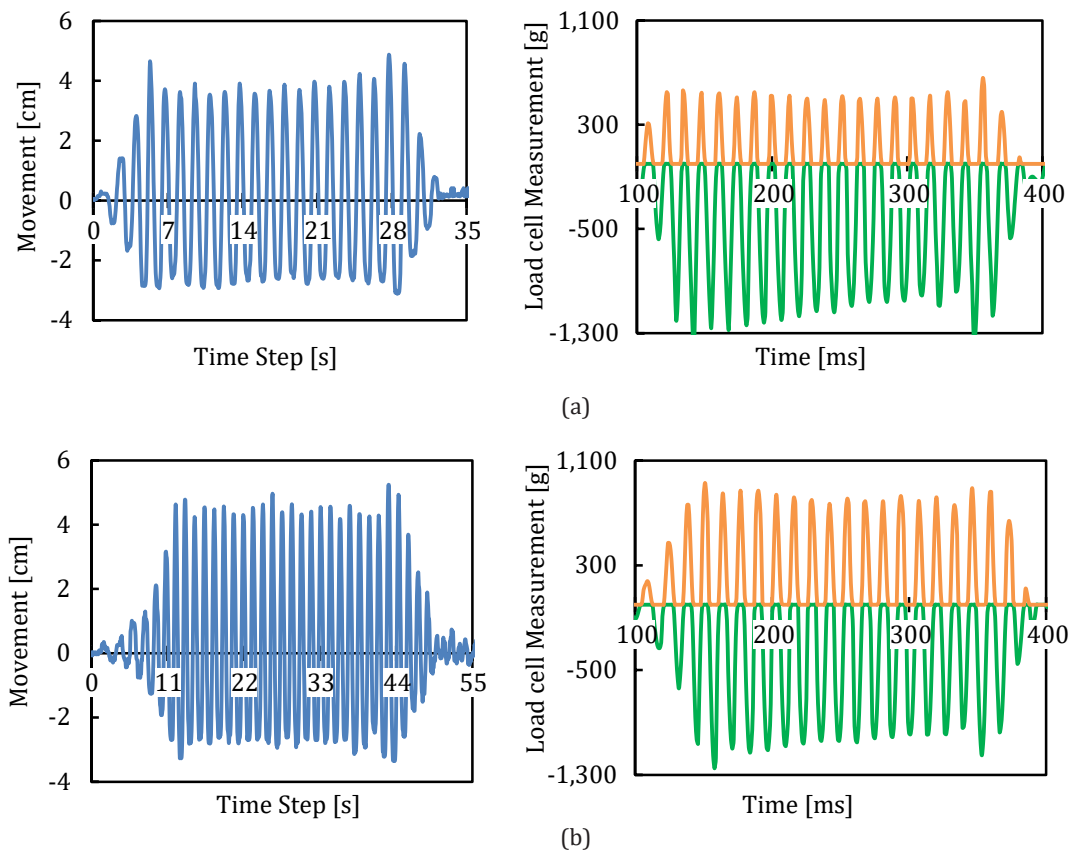


Figure 9 The experimental raw data from variation Floater (a) Type 1 and (b) Type 2.

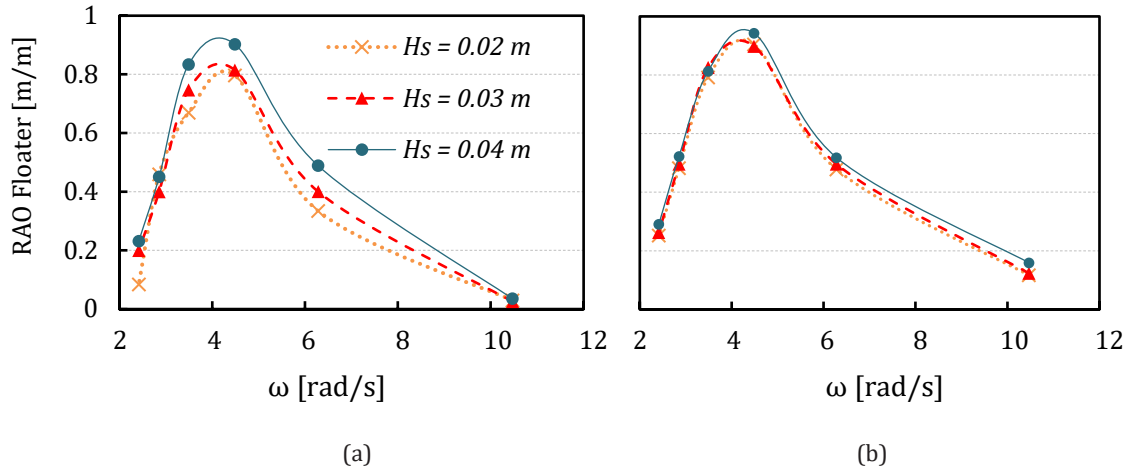


Figure 10 The heave performance of Floater (a) Type 1 and (b) Type 2.

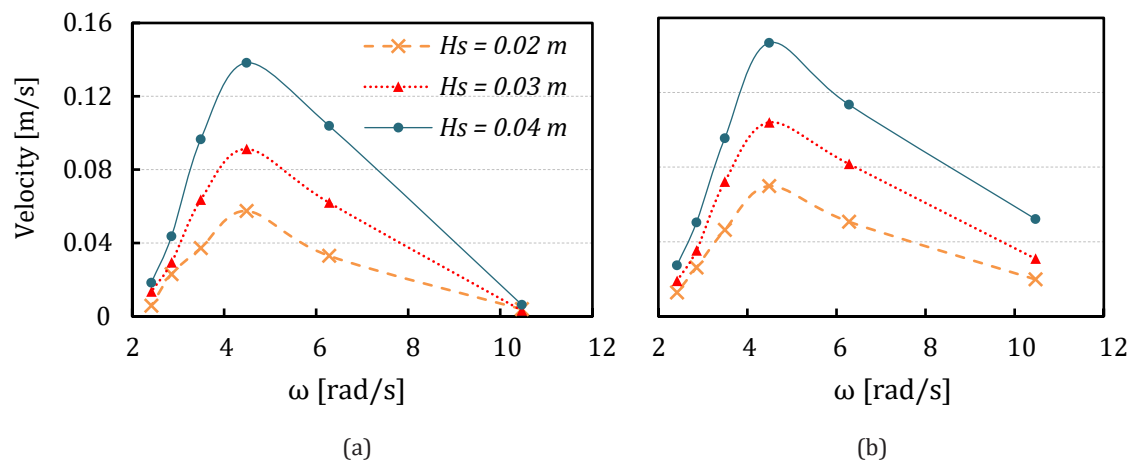


Figure 11 The velocity performance of Floater (a) Type 1 and (b) Type 2.

tured as time series, corresponded to the Point Absorber's motion. To ensure accurate data processing, the raw data was trimmed to focus on the stable segment, and the results of the data are presented in Figure 10. This enabled the generation of a heave performance graph (RAO) using Equation 1. All graphs in Figure 9 below reflect identical wave conditions, with a wave height of 6 cm and a period of 1.4 seconds.

As seen in Figure 10, Floater Type 2 demonstrates a 5% increase in heave performance compared to Floater Type 1. This indicated that a larger floater diameter results in improved heave performance. This aligned with prior study findings [17], which suggested that larger floaters exhibit better performance due to their improved dynamic responses associated with greater diameters. The increased surface area enhanced interaction with wave energy, facilitating greater energy capture and more stable oscillations. These dynamic advantages enabled a more efficient transfer of wave energy to mechanical motion, which was vital to optimize the overall performance of WEC.

However, several factors influenced these results, including floater weight and various dimensional parameters. Prior studies have highlighted that both the weight and the diameter-to-wavelength ratio of the floater significantly affect its response sensitivity, underscoring the need for further research to validate these findings [17]. Notably, despite variations in RAO, both Floater Types exhibited nearly identical average fluctuation velocities, as illustrated in Figure 11. This suggests that while the design dimensions play a crucial role in performance, other parameters must also be considered to fully understand their impact on the system's dynamics.

To calculate the excitation force magnitude, an analytical approach is applied by dividing the force obtained from the experimental method by the wave height, resulting in the graph shown in Figure 12. The graph indicates a 3% increase in excitation force with variations in floater diameter at a wave period of 1.4 seconds. It can be concluded that the excitation force increased as the floater diameter changed. In Figure 12,

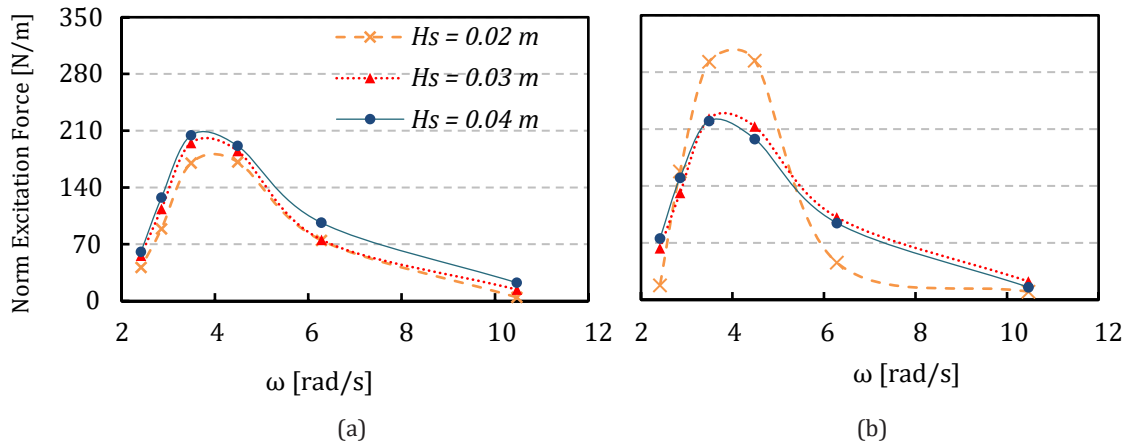


Figure 12 The excitation force magnitude of Floater (a) Type 1 (b) Type 2.

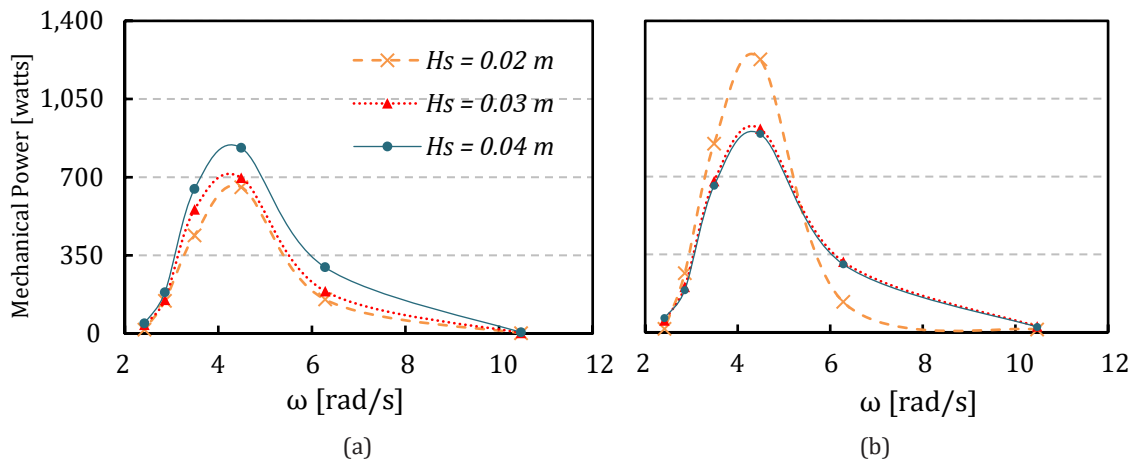


Figure 13 The mechanical power of Floater (a) Type 1 and (b) Type 2.

Norm Excitation Force represents the normalized excitation force, which is obtained by normalizing the excitation force with respect to the corresponding wave height. Through the excitation force data, we obtained the mechanical power graph, as shown in Figure 13.

To calculate mechanical power, analytical calculations based on Equation 6 were crucial. Mechanical power is derived from the excitation force and velocity speed, as shown in Figure 11 and Figure 12 respectively, which presents the results for each variation in floater diameter in Figure 13 (a) and (b). The average mechanical power generated by the two floaters differed by 26.17%, with Floater Type 2 achieving an average of 447 watts, while Floater Type 1 averaged only 330 watts. The highest performance is observed with Floater Type 2 at H_s 0.02 m, reaching 1227 watts. This demonstrated that the floater diameter played a significant role in enhancing performance.

3.2 Numerical Validation

Numerical validation demonstrated good results, as shown in Figure 14, where graphs (a) to (f) illustrate

the performance of RAO, excitation force, and mechanical power. These results highlighted a general consistency in trend lines between the BEM and experimental data. Although BEM tended to overestimate certain values due to viscosity effects, this behavior was commonly observed. Nevertheless, the overall patterns aligned well with experimental observations, indicating reliable and robust numerical performance.

3.3 Numerical Method Results

The numerical simulation results in Figure 15 showed that floater diameter significantly impacted RAO performance. The 31 cm diameter floater achieved the highest peak RAO of approximately 1.9 m/m at 5 rad/s, outperforming the 29 cm floater by about 26.7%. In contrast, the 23 cm floater had the lowest peak RAO of around 1.1 m/m, indicating limited energy absorption. Larger diameters like 33 cm show diminishing returns, with performance slightly declining beyond 5 rad/s. These results emphasized the importance of optimizing floater size to balance energy conversion efficiency and stability.

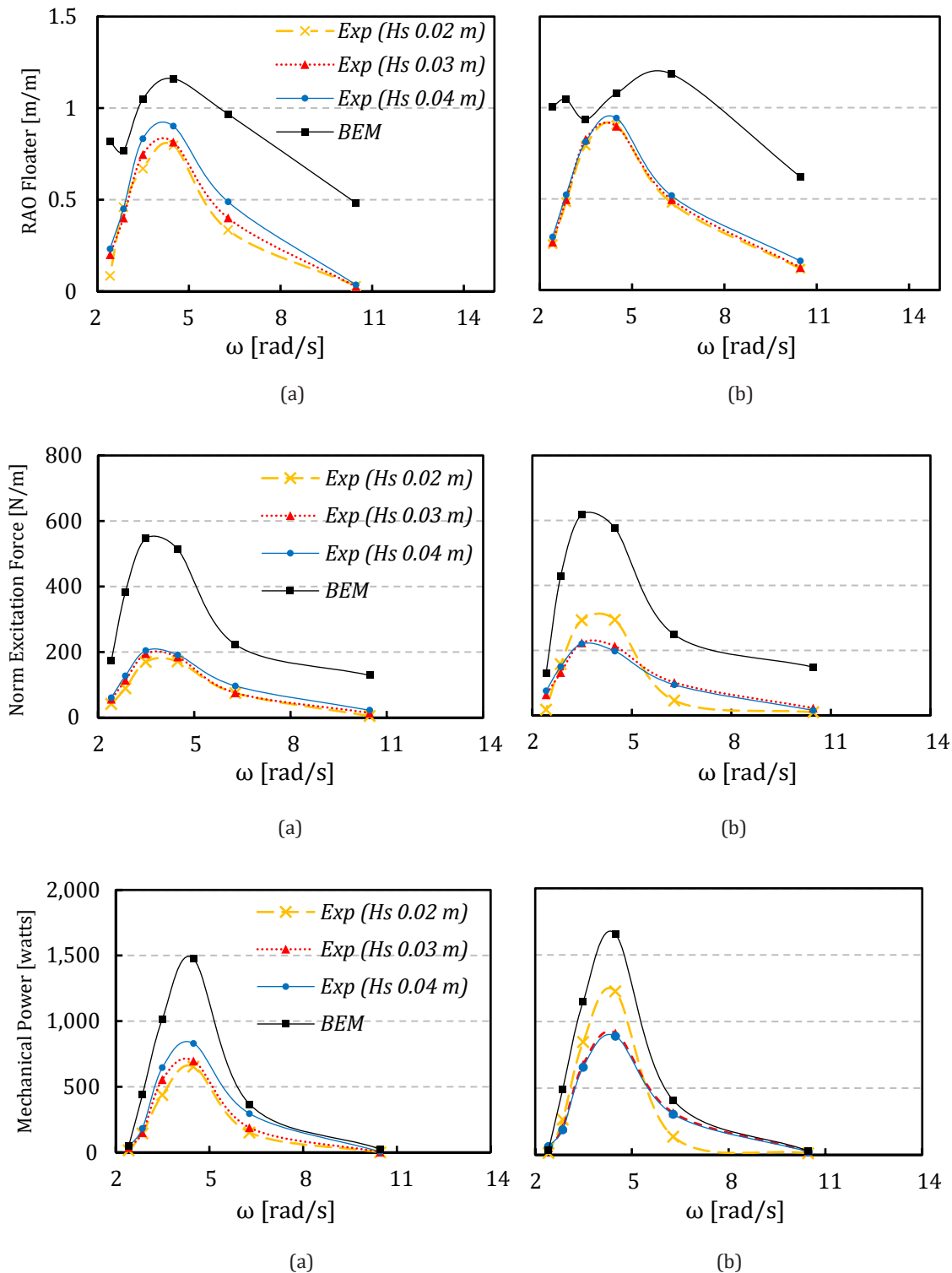


Figure 14 Numerical validation of Floater (a) Type 1 and (b) Type 2.

Based on the heave performance results shown in Figure 15, there was an improvement in performance from a floater diameter of 23 cm to 31 cm. However, the variation with a floater diameter of 33 cm experienced a decrease of 4% at its peak position when compared with

the floater diameter of 31 cm. This suggested that the improvement in floater diameter performance had a limit at a certain value, consistent with prior studies indicated that the optimal floater diameter is typically half the wavelength or an odd multiple of the wavelength [37].

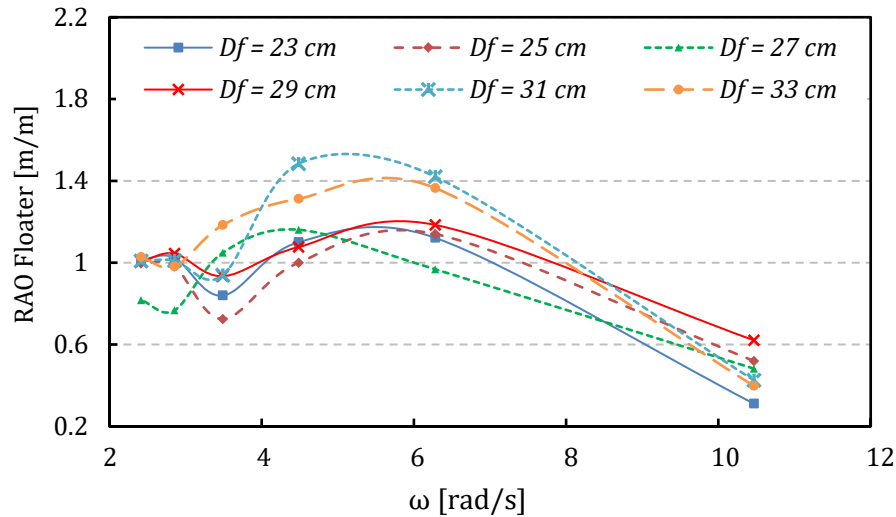


Figure 15 The heave performance results from numerical methods.

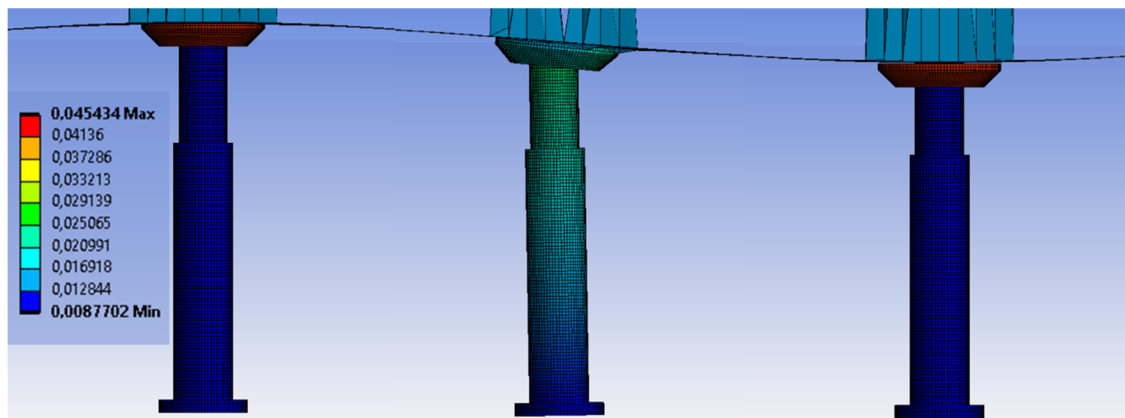


Figure 16 The motion contours of floater and spar at full wave.

Figure 16 observed that the maximum displacement of the floater structure occurred at the wave crest and trough. In contrast, the spar structure exhibited minimal movement at these points, and an oscillation phenomenon was detected between the two structures. During the movement from the wave crest to the trough, the spar structure experienced upward motion, a behavior mirrored in the movement from the wave trough back to the crest. These dynamics highlighted the different response patterns of the floater and spar structures in wave conditions.

The excitation force magnitude with varying floater diameters (D_f) is shown in Figure 17. The variation from 23 cm to 31 cm resulted in a 12% increase in excitation force magnitude. However, the 33 cm diameter showed a decrease. The trend was still the same as shown in Figure 15. The 31 cm floater diameter produced the highest excitation force, but its narrow graph area indicated less ideal performance for wave periods other than the peak.

When comparing the mechanical power shown in Figure 18 representing numerical testing and Figure 13 representing experimental testing, both results converged on the conclusion that the 29 cm diameter (Floater Type 2) performed well. Although the floater with a 31 cm diameter demonstrated an 11.54% superior performance, the 33 cm diameter floater notably exhibited a decline, suggesting that further increasing the diameter might not necessarily enhance performance.

3.4 Annual Energy Production

Figure 19 shows that Floater Type 2 with a 29 cm diameter was selected for further Annual Energy Production (AEP) calculations using Equation 7, as it demonstrated good performance in both methods. To ensure accurate results, the reference was based on experimental testing rather than numerical simulations, which tended to overestimate performance, as shown in

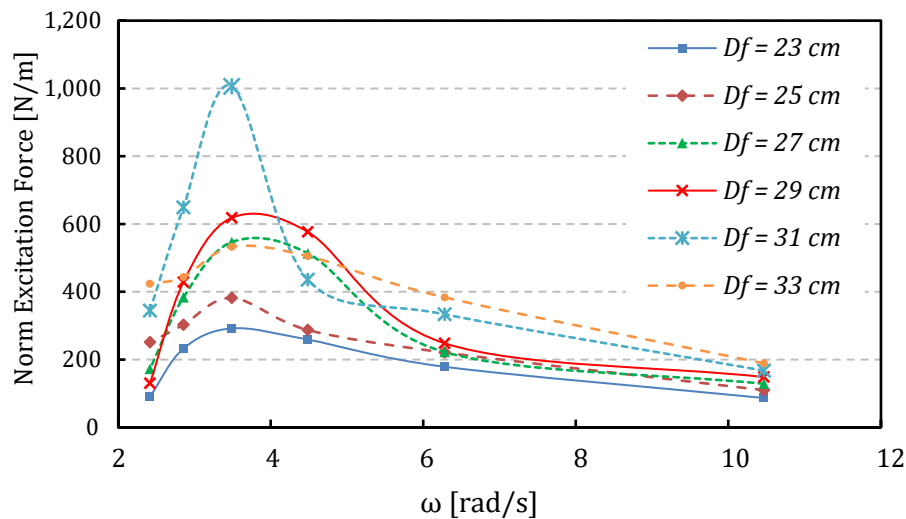


Figure 17 The excitation force magnitude from numerical methods.

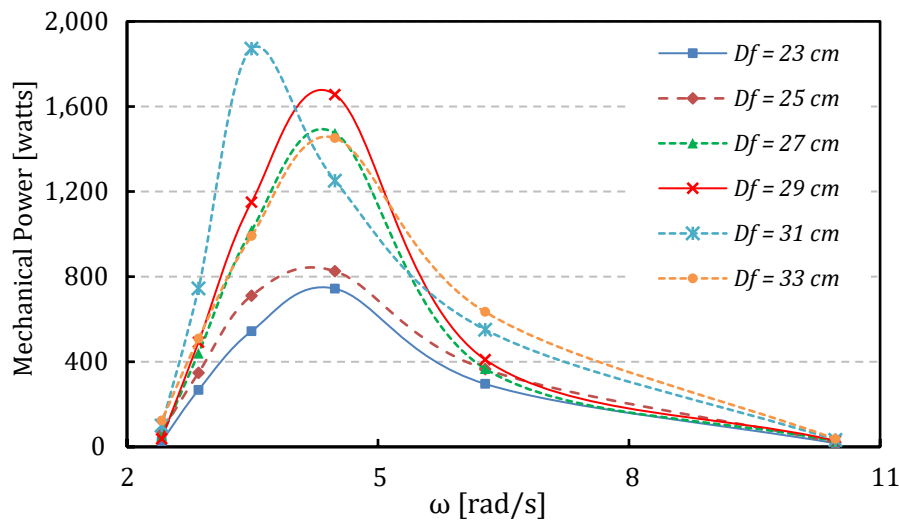


Figure 18 The mechanical power from numerical methods.

Figure 13. The floater's highest output was achieved at a wave height of 0.02 m, producing 497.6 watts, followed by 0.03 m (428.6 watts) and 0.04 m (414.2 watts), with further details provided in Figure 20. These results were then scaled to predict real-world outcomes. As outlined in section 2.2, the WEC model was scaled down by a factor of 1:10 for experimentation. To reflect real-world conditions, the results must be scaled back up accordingly. The laboratory model, derived from the full-scale OPT PowerBuoy, maintains key performance characteristics while ensuring feasibility for testing.

While this study provides valuable insights into the feasibility of WECs technology in Mentawai Waters, certain limitations should be acknowledged. The scaling approach used to estimate full-scale energy production introduces inherent uncertainties, as real-world condi-

tions may involve additional hydrodynamic complexities not fully captured in the experiments or simulations. However, these estimations remain essential as an initial benchmark for assessing the potential energy output and guiding future implementations. Furthermore, while this study primarily focuses on floater diameter variations, other design parameters such as mooring configurations and structural optimizations can be explored in subsequent research to enhance overall performance. The device, designed to operate in an array configuration, achieved an average mechanical power of 446.8 watts. When scaled to full size, this yielded a power output of approximately 35,226 watts, as shown in Figure 20.

The application of this WEC technology can significantly benefit local communities, particularly by providing much-needed lighting in areas without electricity.

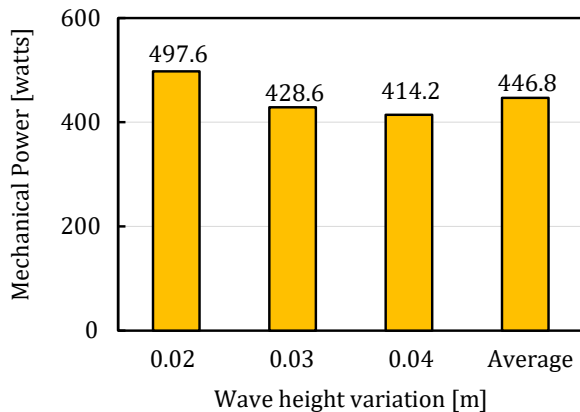


Figure 19 The average power production.

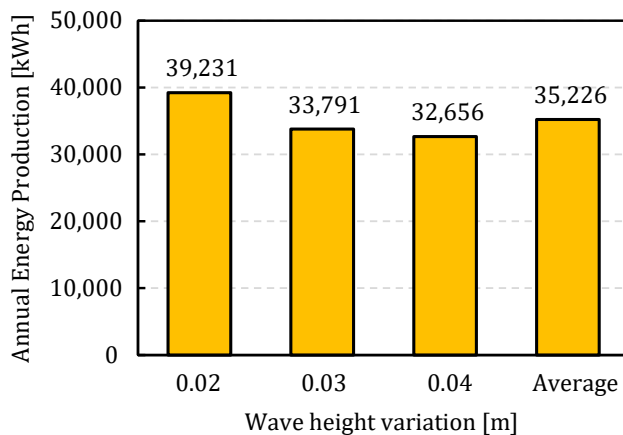


Figure 20 The prediction of annual energy production (for the highest case).

One potential use is the installation of streetlights to improve mobility and safety for residents in remote villages. With each village requiring 20 streetlights, each consuming 200 watts and operating for 10 hours daily (from sunset to dawn), an array of 10 WEC devices using Floater Type 1 can power over 483 streetlights. This can effectively provide lighting for all 23 villages, greatly enhancing local infrastructure and quality of life.

In a previous study focusing on floater height [15], the results were inconsistent, with Floater Type 1 achieving the highest peak performance, while Floater Type 2 had the highest average performance. This suggested that floater height had a limited impact on overall performance. In contrast, the experimental results in this study show that increasing the floater diameter improved performance by 26.17%, indicating that floater diameter played a more crucial role than height variations.

4 Conclusions

This follow-up study evaluates the suitability of WEC technology focusing on the performance of a heaving

device using point absorber mechanisms for Mentawai Waters. The model used adopts the OPT PowerBuoy WEC, selected for its alignment with the region's deep-water and other characteristics. Experimental tests were conducted in the Towing Tank Laboratory at Institut Teknologi Sepuluh Nopember, Surabaya, with two floater configurations Floater Type 1 (27 cm) and Floater Type 2 (29 cm). The experiments were carried out under various wave conditions (H_s : 0.04 m, 0.06 m, 0.08 m; T : 0.6 s to 2.6 s). Additionally, numerical simulations using the BEM method were performed, incorporating additional floater diameter variations (23 cm, 25 cm, 31 cm, and 33 cm) for comparison with the experimental setup. Both the experimental and numerical results consistently showed that Floater Type 2, with a diameter of 29 cm, outperformed the other configurations, providing the best heave performance, excitation force, and mechanical power output. This was demonstrated by the average mechanical power generated by Floater Type 2, which was 447 watts, while Floater Type 1 only averaged 330 watts, a 26.17% difference. The full-scale AEP prediction for the WEC system in Mentawai Waters reached a maximum of 35,226 kWh. This scaling approach has inherent uncertainties due to unmodeled real-world hydrodynamic complexities but remains a useful reference for initial assessment. Based on these findings, an array of 10 WEC units is recommended, capable of illuminating 23 villages, each with 20 streetlights rated at 200 watts, with Floater Type 2 as the most suitable configuration for maximizing energy output.

Acknowledgments: The authors would like to convey their appreciation to Institut Teknologi Sepuluh Nopember, which funded the current project under a scheme called Scientific Research under contract number 1628/ PKS/ITS/2024.

Author Contributions Statement: Conceptualization, Methodology, Formal Analysis, Writing Original Draft, Writing Review and Editing, Funding Acquisition, Dendy Satrio; Investigation, Data Curation, Visualization, Writing Original Draft, Febri Budihantono, Mohammad Farid; Formal Analysis, Review and Editing, Nik Ahmad Ridhwan, Maktum Muharja, Muhammad Luqman Hakim, Tuswan; Writing Review and Editing, Dandun Maheesa Prabowoputra, Fuad Mahfud Assidiq, Wahyu Nur Fadilah.

References

- [1] BPS (Indonesian Central Statistics Agency), "Indonesia's mid-year population," Jakarta, 2020.
- [2] (Ministry of Energy and Mineral Resources of the Republic of Indonesia) KESDM, "ESDM Sector Performance Achievements in 2023 and Targets for 2024," Jakarta, 2024.

- [3] ESDM, "Indonesia Energy Outlook 2021," 2021.
- [4] H. I. Suherman and P. Raharjo, "Ocean Wave Energy Potential in the Mentawai Waters," vol. 18, no. 2, pp. 97–110, 2020, doi: <http://dx.doi.org/10.32693/jgk.18.2.2020.564>.
- [5] Mukhtasor et al., "PETA POTENSI ENERGI LAUT INDONESIA," 2014.
- [6] D. Satrio et al., "A Numerical Study of the Effect of Depth Immersion and Rotation Direction on the Performance of Cross-Flow Savonius Turbines," *Pomorstov*, vol. 38, no. 2, pp. 250–262, 2024, doi: <https://doi.org/10.31217/p.38.2.7.A>.
- [7] E. Erwandi et al., "Numerical Analysis of Resistance and Motions on Trimaran Floating Platform for Tidal Current Power Plant," *Int. Rev. Model. Simulations*, vol. 17, no. 1, pp. 6–16, 2024, doi: [10.15866/iremos.v17i1.24366](https://doi.org/10.15866/iremos.v17i1.24366).
- [8] D. Satrio, Suntoyo, H. B. Widyawan, M. A. Ramadhani, and M. Muharja, "Effects of the distance ratio of circular flow disturbance on vertical-axis turbine performance: An experimental and numerical study," *Sustain. Energy Technol. Assessments*, vol. 63, no. March 2024, p. 103635, 2024, doi: [10.1016/j.seta.2024.103635](https://doi.org/10.1016/j.seta.2024.103635).
- [9] S. Musabikha et al., "The effects of flow rate on impedance measurements of marine coatings using a rotating cylinder electrode," *J. Coatings Technol. Res.*, pp. 1–12, 2024, doi: [10.1007/s11998-024-00957-w](https://doi.org/10.1007/s11998-024-00957-w).
- [10] D. Satrio et al., "The Advantages and Challenges of Carbon Fiber Reinforced Polymers for Tidal Current Turbine Systems – An Overview," in *IOP Conf. Series: Earth and Environmental Science*, Surabaya: IOP Publishing, 2024, p. 1298. doi: [10.1088/1755-1315/1298/1/012029](https://doi.org/10.1088/1755-1315/1298/1/012029).
- [11] Rasgianti, Mukhtasor, and D. Satrio, "The Influence of Structural Parameters on the Ultimate Strength Capacity of a Designed Vertical Axis Turbine Blade for Ocean Current Power Generators," *Sustain.*, vol. 16, no. 7655, pp. 1–24, 2024, doi: <https://doi.org/10.3390/su16177655>.
- [12] IRENA, *Innovation outlook: Ocean energy technologies*. 2020.
- [13] IRENA, *SCALING UP INVESTMENTS IN OCEAN ENERGY TECHNOLOGIES*. 2023.
- [14] D. Magagna, *Ocean energy : technology development report 2018*. 2018. doi: [10.2760/158132](https://doi.org/10.2760/158132).
- [15] D. Satrio et al., "Technical Feasibility of Implementing Heaving Device Wave Energy Converter: A Case Study in Mentawai Waters , Indonesia," *Mar. Syst. Ocean Technol.*, pp. 1–17, 2024, doi: [10.1007/s40868-024-00151-y](https://doi.org/10.1007/s40868-024-00151-y).
- [16] S. J. Beatty, M. Hall, B. J. Buckham, P. Wild, and B. Bocking, "Experimental and numerical comparisons of self-reacting point absorber wave energy converters in regular waves," *Ocean Eng.*, vol. 104, pp. 370–386, 2015, doi: [10.1016/j.oceaneng.2015.05.027](https://doi.org/10.1016/j.oceaneng.2015.05.027).
- [17] C. Zhao, F. Cao, and H. Shi, "Optimisation of heaving buoy wave energy converter using a combined numerical model," *Appl. Ocean Res.*, vol. 102, no. May, p. 102208, 2020, doi: [10.1016/j.apor.2020.102208](https://doi.org/10.1016/j.apor.2020.102208).
- [18] A. Rahimi, S. Rezaei, J. Parvizian, S. Mansourzadeh, and J. Lund, "Numerical and experimental study of the hydrodynamic coefficients and power absorption of a two-body point absorber wave energy converter," *Renew. Energy*, vol. 201, no. P1, pp. 181–193, 2022, doi: [10.1016/j.renene.2022.10.103](https://doi.org/10.1016/j.renene.2022.10.103).
- [19] M. H. Fakhri, D. Satrio, and Suntoyo, "Numerical analysis of drag coefficient for damping plate on the submerged body of two-body point absorber device as wave energy converter," in *International Conference on Green Energy, Computing and Intelligent Technology (GEn-CITY 2023)*, IEEE Xplore, 2023. doi: [10.1049/icp.2023.1784](https://doi.org/10.1049/icp.2023.1784).
- [20] M. Zikra, "Preliminary Assessment of Wave Energy Potential around Indonesia Sea," *Appl. Mech. Mater.*, vol. 862, pp. 55–60, 2017, doi: [10.4028/www.scientific.net/amm.862.55](https://doi.org/10.4028/www.scientific.net/amm.862.55).
- [21] S. Rahma Utami, "Potential Study of Sea Wave Power System Using Oscillating Water Column (OWC) in Thirty Marine Areas Indonesia. (Bahasa Indonesia)," *Tek. Elektro*, 2010.
- [22] N. F. Marelsa and Y. Oktaviandra, "Analisis Karakteristik Gelombang Laut Menggunakan Software Windwave-12 (Studi Kasus: Kepulauan Mentawai)," *Oseana*, vol. 44, no. 2, pp. 10–24, 2019, doi: [10.14203/oseana.2019.vol.44no.2.23](https://doi.org/10.14203/oseana.2019.vol.44no.2.23).
- [23] A. F. d. O. Falcão, "Wave energy utilization: A review of the technologies," *Renew. Sustain. Energy Rev.*, vol. 14, no. 3, pp. 899–918, 2010, doi: [10.1016/j.rser.2009.11.003](https://doi.org/10.1016/j.rser.2009.11.003).
- [24] Y. Zhang, Y. Zhao, W. Sun, and J. Li, "Ocean wave energy converters: Technical principle, device realization, and performance evaluation," *Renew. Sustain. Energy Rev.*, vol. 141, pp. 110–764, May 2021, doi: [10.1016/j.rser.2021.110764](https://doi.org/10.1016/j.rser.2021.110764).
- [25] J. van Rij, Y. H. Yu, K. Edwards, and M. Mekhiche, "Ocean power technology design optimization," *Int. J. Mar. Energy*, vol. 20, pp. 97–108, 2017, doi: [10.1016/j.ijome.2017.07.010](https://doi.org/10.1016/j.ijome.2017.07.010).
- [26] OPT, "PB3 PowerBuoy."
- [27] M. A. Chatzigiannakou, I. Dolguntseva, and M. Leijon, "Off-shore deployments of wave energy converters by sea-based industry AB," *J. Mar. Sci. Eng.*, vol. 5, no. 2, pp. 1–11, 2017, doi: [10.3390/jmse5020015](https://doi.org/10.3390/jmse5020015).
- [28] P. Malali and K. Marchand, "Assessment of currently available ocean wave energy conversion systems using technology readiness levels," *Int. J. Renew. Energy Technol.*, vol. 11, no. 2, p. 126, 2020, doi: [10.1504/ijret.2020.108332](https://doi.org/10.1504/ijret.2020.108332).
- [29] SeaBased, "SeaBased."
- [30] A. G. Majidi, B. Bingölbalı, A. Akpınar, G. Iglesias, and H. Jafali, "Downscaling wave energy converters for optimum performance in low-energy seas," *Renew. Energy*, vol. 168, pp. 705–722, 2021, doi: [10.1016/j.renene.2020.12.092](https://doi.org/10.1016/j.renene.2020.12.092).
- [31] P. D. I. Torino, "MASTER 'S DEGREE IN NUCLEAR AND ENERGY Advancements in wave energy conversion : a numerical analysis of the C4 CorPower WEC' s dynamic response in various wave scenarios," no. March, 2024.
- [32] JEC, "Corpower's wave energy concept."
- [33] TETHYS, "WaveNET Wave Energy Converter Array."
- [34] W. Edwards, D. Findlay, D. Scott, and P. Graham, "SHAPE Pilot Albatern: Numerical Simulation of Extremely Large Interconnected Wavenet Arrays," no. Figure 1, pp. 1–8, 2014.
- [35] OPT, "PB3 PowerBuoy® – Ocean Power Technologies." 2021.
- [36] Aston et al., "Harnessing Wave Energy to Provide Autonomous Offshore Power for Subsea Well Monitoring," in *Off-shore Technology Conference*, 2022. doi: <https://doi.org/10.4043/31749-MS>.
- [37] P. A. Lynn, *Electricity from Wave and Tide*. 2014.
- [38] The European Marine Energy Centre Ltd, "Guidelines for Design Basis of Marine Energy Conversion Systems," 2009.